Pergamon

Corrosion Science, Vol. 40, No. 9, pp. 1547–1560, 1998

Printed in Great Britain.
0010–938X/98/$—see front matter

PII: S0010-938X(98)00066-3

MECHANISMS OF FORMATION AND STRUCTURE OF GREEN RUST ONE IN AQUEOUS CORROSION OF IRON IN THE PRESENCE OF CHLORIDE IONS

PH. REFAIT, M. ABDELMOULA and J.-M.R. GÉNIN

Laboratoire de Chimie Physique pour l'Environnement, UMR 7564 CNRS-Université. Henri Poincaré-Nancy 1, Equipe sur la Réactivité des Espèces du Fer & Département Science des Matériaux, ESSTIN, Univ. H. Poincaré, 405, rue de Vandoeuvre, F-54600 Villers-lès-Nancy, France

Abstract—The crystal structure of the Fe(II)-Fe(III) hydroxychloride known as Green Rust one (GR) was investigated by X-ray diffraction and confirmed to be analogous with that of iowaite. It is a rhombohedral crystal [$R\bar{3}m$, $a = 0.3190(1)$ nm, $c = 2.385(6)$ nm] consisting of $Fe(OH)_2$ like-hydroxide sheets which alternate regularly with interlayers composed of Cl^- ions and H_2O molecules and follow the stacking sequence *AcBiBaCjCbAk* . . . , where *A*, *B*, *C* are OH^- layers, *a*, *b*, *c* Fe layers and *i*, *j*, *k* interlayers. By means of transmission Mössbauer spectroscopy analyses at 20 K of the solid phases formed during the oxidation of $Fe(OH)_2$ into $GR(Cl^-)$, it was demonstrated that the composition of the GR compound varied continuously from $Fe^{II}_3Fe^{III}(OH)_8Cl \cdot nH_2O$, with *n* probably equal to 2, to approximately $Fe^{II}_{2.2}Fe^{III}(OH)_{6.4}Cl \cdot nH_2O$. The formation of $GR(Cl^-)$ involves an *in situ* incorporation of the Cl^- ions from the solution into the interlayers of $GR(Cl^-)$ and a corresponding oxidation of Fe(II) to Fe(III) without any structural changes. This mechanism, which allows the oxidation of iron at the only cost of chloride intercalation, explained why GR formation would be favoured *vs* other possibilities such as direct ferric oxyhydroxide or magnetite formation. To confirm this assumption, *in situ* transmission Mössbauer spectroscopy analyses were performed on iron coupons polarised potentiostatically in KCl solutions of pH about 9. At a potential of $-0.55\,V_{SHE}$ a ferrous hydroxide layer is formed on the metal while at $-0.35\,V_{SHE}$ the corrosion product is mainly composed of GR.

Keywords: A. Fe(II)-Fe(III) hydroxychloride, A. Green Rust, B. potentiostatically induced corrosion, B. Mössbauer spectroscopy, C. crystal structure, C. Pourbaix diagram.

INTRODUCTION

Green Rusts (GRs) are unstable Fe(II)-Fe(III) hydroxy-salts which oxidise in the presence of oxygen. They are transient compounds between metallic iron and final corrosion products, and therefore may govern the mechanisms and kinetics of corrosion and passivation of iron-based alloys in aqueous media. Due to their instability, their identification as corrosion products of iron and steel was rarely reported. Anyhow, many works indicate that GRs can form easily in a wide range of experimental conditions [1–10].

The chloride-containing Green Rust, $GR(Cl^-)$, should be one of the most commonly occurring GR compound resulting from iron corrosion, owing to the abundance of chloride

Manuscript received 9 December 1997; accepted 7 March 1998.

ions in various environments and to its well known aggressivity. Studies were performed aiming at the determination of its composition, which leads to the idealised formula of $Fe^{II}_3Fe^{III}(OH)_8Cl\cdot nH_2O$ since a Fe(II)/Fe(III) ratio of 3 was observed and n is probably equal to 2 [11–13]. Nevertheless, it was also noted that the composition could vary [11, 13, 14] since the Fe(II)/Fe(III) ratio decreases down to about 2 as the chloride concentration of the aqueous media increases [14]. The standard free enthalpy of formation of $Fe^{II}_3Fe^{III}(OH)_8Cl\cdot nH_2O$ could also be determined [12, 15] and potential E *vs* pH equilibrium diagrams were drawn for α-iron in chloride-containing aqueous media taking into account the afferent GR compound. Comparing the equilibrium conditions between α-Fe and $GR(Cl^-)$, given by $E_{GR} = -0.119 - 0.525\,pH - 0.0066\,\log[Cl^-]$ [12] with those between α-Fe and Fe_3O_4, $E_M = -0.085 - 0.0591\,pH$ [16], it can be seen that $GR(Cl^-)$ is metastable with respect to magnetite as soon as the pH is over ~ 5, since E_{GR} becomes greater than E_M for $[Cl^-] < 1$. In order to understand under which conditions $GR(Cl^-)$ will be formed preferentially to magnetite or other iron oxides and/or oxyhydroxides, it would be necessary to precise the mechanisms of its formation.

In this article, it is intended to demonstrate that $GR(Cl^-)$ can be obtained by cathodic polarisation of α-iron, direct precipitation from dissolved ferrous and ferric salts, and by aerial oxidation of ferrous hydroxide as well. The mechanisms of formation of $GR(Cl^-)$ are interpreted in view of its crystal structure.

EXPERIMENTAL

Preparation of GR precipitates by oxidation of $Fe(OH)_2$

$GR(Cl^-)$ is usually prepared by aerial oxidation of ferrous hydroxide suspensions in the presence of a slight excess of dissolved ferrous chloride [11, 12, 17, 18]. 100 ml of a solution of 0.40 mol l^{-1} of NaOH were added to 100 ml of a solution of 0.23 mol l^{-1} of $FeCl_2\cdot 4H_2O$; thus, 0.2 mol l^{-1} of $Fe(OH)_2$ was precipitated, leaving in solution an excess of 0.03 mol l^{-1} of dissolved ferrous chloride. Magnetic stirring ($\sim$500 rpm) in the open air ensured a progressive homogeneous oxidation of the precipitate and a thermostat controlled the temperature, kept at 25 ($\pm$0.5)°C. Reactions were monitored by recording the potential E of a platinum electrode dipped in solution, using the saturated calomel electrode as reference (but all potentials in the following refer to the standard hydrogen electrode, SHE). The solid phases were analysed by transmission Mössbauer spectroscopy, TMS, at 20 K at various stages of the reaction, from the initial precipitation of $Fe(OH)_2$ to its complete transformation into $GR(Cl^-)$. The samples were filtrated and prepared for TMS measurements under inert N_2 atmosphere and placed in a cryostat at low temperature under an inert He atmosphere for preventing any unwitting oxidation. The temperature of 20 K was chosen so as to discriminate clearly $Fe(OH)_2$ from $GR(Cl^-)$, since $Fe(OH)_2$ is magnetically ordered under the Néel temperature of 34 K [19], whereas GRs remain paramagnetic down to 15 K [20, 21]. To achieve analyses at such a temperature, a closed Mössbauer cryogenic workstation with vibrations isolation stand manufactured by Cryo Industries of America® was used. Helium exchange gas thermally coupled the sample to the refrigerator in order to operate down to 15 K.

Direct precipitation of $GR(Cl^-)$

Since mixed M(II)-M′(III) pyroaurite-like hydroxysalts can be prepared by coprecipitation from M(II) and M′(III) salts [22–24], a new and simplest way of preparing

GR(Cl^-) was attempted, by means of a direct precipitation from ferrous and ferric salts. Aqueous solutions of ferrous chloride, ferric chloride and caustic soda were mixed, with a NaOH concentration of $1\,mol\,l^{-1}$, a ratio $\{[FeCl_2]+[FeCl_3]\}/[NaOH]$ of 0.6 and a $[FeCl_2]/[FeCl_3]$, that is Fe(II)/Fe(III) ratio of 3. The resulting green precipitate was immediately analysed by TMS at 20 K without allowing any oxidation.

Electrochemical cell for in situ *Mössbauer spectroscopy*

Electrochemical experiments were performed by use of a three electrodes cell designed specifically for TMS measurements. The reference electrode was a saturated calomel electrode and the counter electrode a platinum wire. A Radiometer PGP-201® potentiostat monitored by means of the VoltaMaster-1® software was used for potentiostatic experiments. The $9\,cm^2$ working electrodes were prepared from $50\,\mu m$ foil of α-Fe (99.5 min.) provided by Goodfellow®. They were immersed in a $1\,mol\,l^{-1}$ KCl solution with a pH of 9. The electrochemical cell, previously devised by Chanson *et al.* [25] for the study of the electrochemical behaviour of iron in strongly alkaline solution was adapted to our purpose. The cell was designed in order that the thickness of the electrolyte crossed by the gamma ray beam was as thin as possible using two adjustable teflon windows. The body of the cell was made from a plexiglas block. Viton seals were pressed onto the windows and their support by stainless steel joiner-cramps. The lid of the cell was easily removable which allowed the setting of the various electrodes. The TMS device was a constant-acceleration Mössbauer spectrometer with a 25 mCi source of ^{57}Co in Rh. The velocity was calibrated with a $25\,\mu m$ foil of α-Fe and all experiments were performed at room temperature.

X-ray diffraction analysis

The samples to be analysed by X-ray diffraction (XRD) were filtered, dried 12 hours in a glove bag under nitrogen and ground to powder. They were then poured into Lindemann glass tubes (2 mm diameter and 0.01 mm thick) which were sealed immediately after. The study was performed with a classical vertical axis counter diffractometer. A 1 kW Mo source was used and a quartz monochromator with a long focalisation distance (570 mm) gave an angular resolution $\Gamma_{(FWHM)} = 0.04^\circ$ (θ). However, it was increased up to 0.08° by the thickness of the used Lindemann glass. As a complementary technique, the diffraction pattern was recorded using a Curve Position Sensitive Detector (CPS 120 INEL®) placed in horizontal position, using a rotating anode X-ray generator (11.4 kW). The sample was set in the centre of the diffractometer, in the rotating crystal condition.

RESULTS

TMS monitoring at 20 *K of the formation of GR(Cl^-) by aerial oxidation of Fe(OH)$_2$*

The evolution with time of the redox potential E during the oxidation reaction of a $Fe(OH)_2$ suspension can be described as follows (Fig. 1): E stays approximately constant during thirty minutes, then increases continuously before reaching a maximum. This first part corresponds to the transformation of $Fe(OH)_2$ into GR [12]. In the second part, E decreases, reaches a plateau and then increases again. This corresponds to the oxidation of the GR into ferric oxyhydroxides and/or magnetite [12]. Five samplings were made during the first reaction stage, when $Fe(OH)_2$ was oxidising into GR(Cl^-). The precipitates were then analysed by TMS at 20 K (Fig. 1 and Table 1).

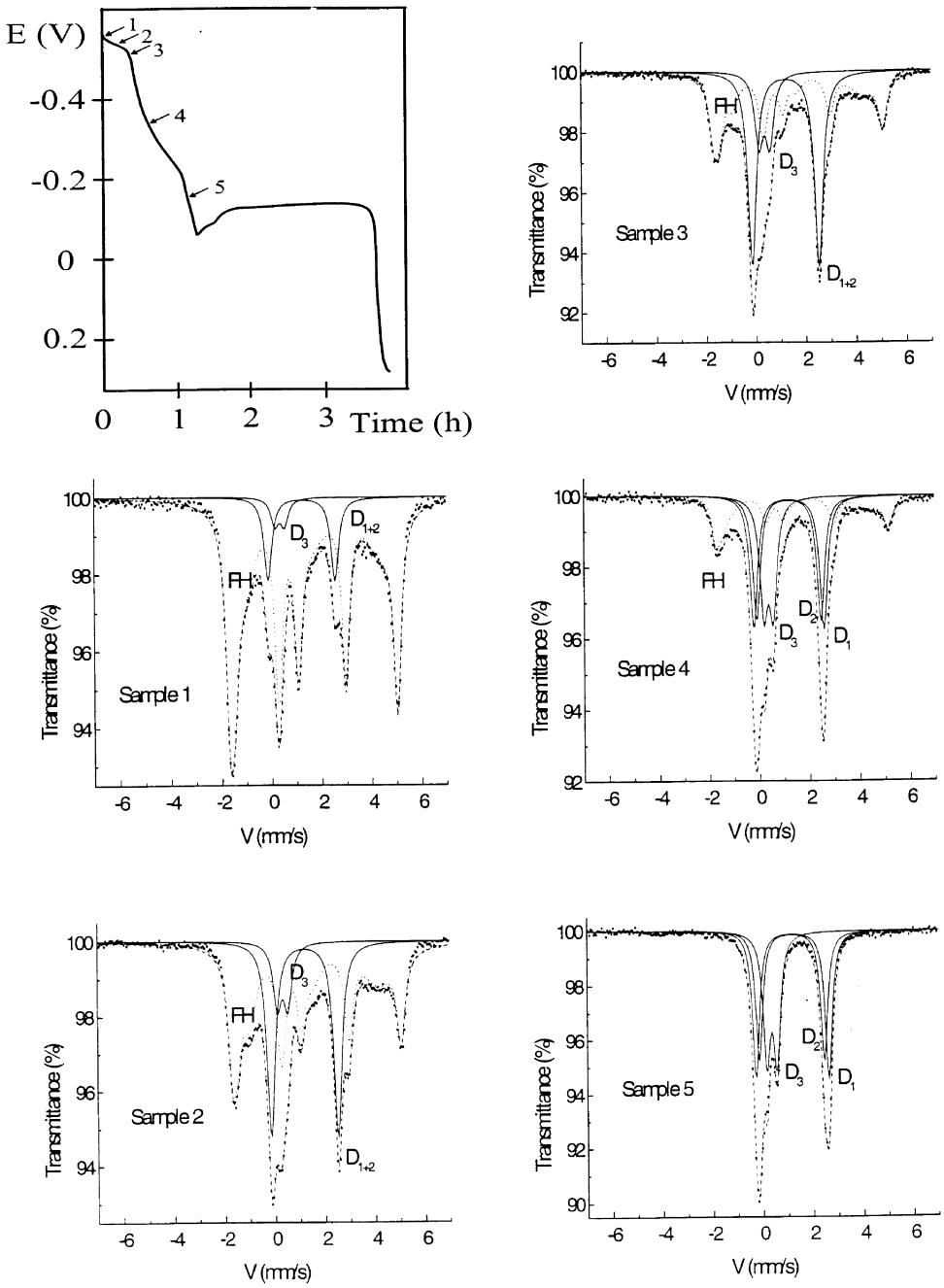

Fig. 1. Mössbauer spectra measured at 20 K of samples 1 to 5, at various stages of the oxidation of ferrous hydroxide into GR(Cl^-) and corresponding *E vs* time curve showing the location of the various samplings (the potential axis is downward). TMS: ··· experimental curve; ——— elementary quadrupole doublets; – – – global computed curve.

Table 1. TMS analyses at 20 K of samples 1–5, at various stages of the oxidation of ferrous hydroxide into GR(Cl^-); composition of the sample and hyperfine parameters of the GR compound

	Sample 1			Sample 2		
% $Fe(OH)_2$		86.8			62.8	
% GR		13.2			37.2	
GR sites	δ	ΔE_Q	RA	δ	ΔE_Q	RA
D_{1+2}	1.32	2.66	10	1.31	2.65	28.3
D_3	0.46	0.38	3.2	0.45	0.41	8.9

	Sample 3			Sample 4			Sample 5		
% $Fe(OH)_2$		44.2			25.1			0	
% GR		55.8			74.9			100	
GR sites	δ	ΔE_Q	RA	δ	ΔE_Q	RA	δ	ΔE_Q	RA
D_1	1.31	2.75	22.5	1.31	2.78	27.3	1.31	2.89	37
D_2	1.31	2.57	19.6	1.31	2.55	25.5	1.29	2.57	32
D_3	0.52	0.39	13.7	0.52	0.37	22.1	0.40	0.40	31

δ = isomer shift with respect to metallic α-iron in mm s^{-1}; ΔE_Q = quadrupole splitting in mm s^{-1}; RA = relative abundance in %. Widths are constrained to be equal for each Lorentzian-shape line.

The spectrum of magnetically ordered ferrous hydroxide is composed of eight lines as due to the coupling of a large quadrupole splitting with a small hyperfine field [19, 26]. According to a theoretical treatment [21], two of these lines should overlap, and the spectrum would have been fitted with only seven lines. However, some additional peaks were to be used, indicating that the compound was not pure ferrous hydroxide. This confirms a previous study based on TMS analysis at 78 K [27, 28] and is interpreted as the consequence of the presence of a few percents of chloride ions substituted for OH^- ions in the hydroxide lattice. In such chloride-containing ferrous hydroxides, $Fe(OH)_{2-x}Cl_x$ [27, 28], there exist two iron sites, the first one identical to what is found in pure $Fe(OH)_2$, that is an iron atom in the centre of an octahedron made of 6 OH^- ions, the second one corresponding to an iron atom in an octahedron built on 5 OH^- ions and 1 Cl^- ion. The spectrum of GR(Cl^-) at 20 K remained that of a paramagnetic compound. It is essentially composed of two quadrupole doublets D_{1+2} and D_3, but the computer fittings were in most cases more reliable with D_{1+2} splitted in two distinct doublets D_1 and D_2. D_1 and D_2 are due to the Fe(II) cations inside GR whereas D_3 is due to the Fe(III) cations [12]; the $(D_1+D_2)/D_3$ ratio measures the overall Fe(II)/Fe(III) ratio of the compound.

Sample 1, taken about one minute after precipitation is essentially made of ferrous hydroxide, but GR(Cl^-) already appears in a non-negligible proportion, about 13%. As the oxidation goes on, the proportion of GR(Cl^-) increases at the expense of that of ferrous hydroxide, until all $Fe(OH)_2$ is consumed (sample 5). Two stages must be distinguished, relating to the composition of the GR. In a first step of the oxidation, the composition remains constant, corresponding to a Fe(II)/Fe(III) ratio of 3 (samples 1–3). Simultaneously, the redox potential of the solution stays approximately constant. In a second part, the composition of GR(Cl^-) varies and its Fe(II)/Fe(III) ratio decreases down to 2.23 at the end of the reaction, i.e. for sample 5. In this case, the redox potential increases continuously.

Precipitation of GR(Cl^-) from ferrous and ferric chlorides

The TMS spectrum at 20 K (Fig. 2) of the precipitate obtained is clearly that of GR(Cl^-). The hyperfine parameters of the three quadrupole doublets are similar to those obtained for samples 1–5 described above. D_1, D_2 and D_3 have quadrupole splitting values ΔE_Q of 2.82, 2.52 and 0.37 mm s^{-1} and relative abundances of 35, 37 and 28%, respectively. Therefore, Fe(II)-Fe(III) oxides with spinel structure, similar to magnetite, are not obtained when the Fe(II)/Fe(III) ratio is large, while they usually result from such coprecipitation syntheses when the Fe(II)/Fe(III) ratio is lower than 0.5 [29].

Electrochemically induced corrosion of iron in KCl solutions

An E vs pH Pourbaix diagram of iron in chloride containing aqueous solution was drawn (Fig. 3) for a Cl^- activity similar to that of a 1 M KCl solution, i.e. $a[Cl^-] \approx 0.55$ if computed by extended Debye-Hückel law: $-\log \gamma_i = [0.51 Z_i^2 \sqrt{I}]/[1 + a_i^0 0.33 \times 10^8 \sqrt{I}]$ with an ionic strength $I = 1$, an effective diameter $a_i^0 = 3.0 \times 10^{-8}$ for $i = Cl^-$. In this diagram, the chloride-containing GR was taken into account by using the standard free enthalpy of formation estimated previously [15]. Its chemical formula was set at $Fe_4(OH)_8Cl \cdot nH_2O$ [11, 12, 30], that is the composition of the GR which forms initially from ferrous hydroxide. Two potential values were chosen accordingly, the first one at -0.55 V, the second one at -0.35 V. At the pH values considered here, about 9, the first point is thus located in the domain of $Fe(OH)_2$ and the second point in the domain of GR(Cl^-) ($\oplus$ in Fig. 3). The TMS spectra (Fig. 4) were obtained after 4 days of polarisation. The spectrum corresponding to $E = -0.55$ V could be obtained *in situ* in

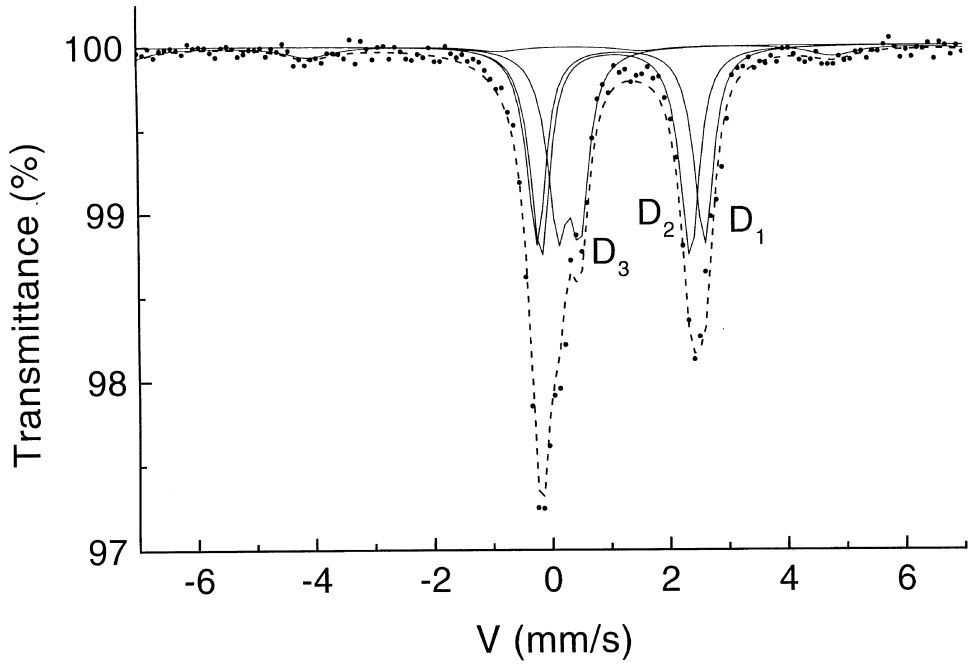

Fig. 2. Mössbauer spectrum measured at 20 K of GR(Cl^-) precipitated from ferrous and ferric chloride solutions. ··· experimental curve; ——— elementary quadrupole doublets; —- global computed curve.

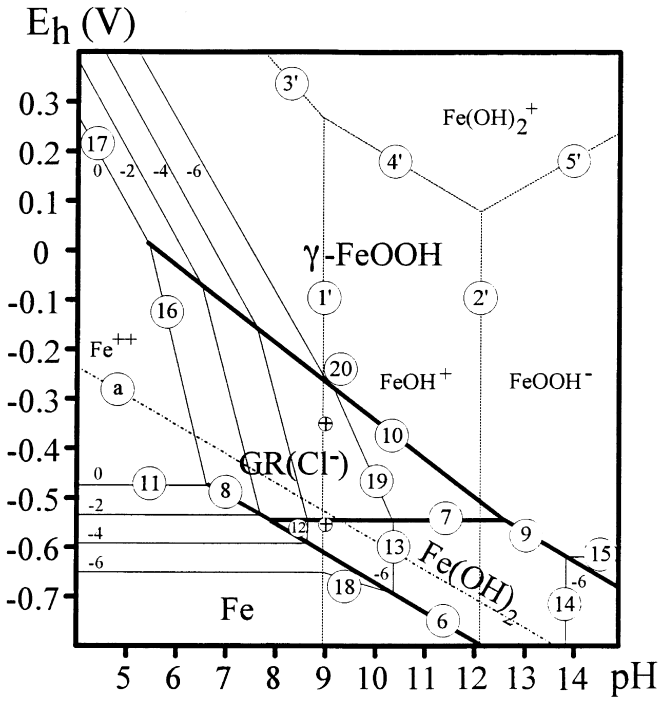

Fig. 3. *E*-pH equilibrium diagram of the system Fe/chloride containing solution at 25°C for an activity $a[Cl^-] = 0.55$, corresponding to a 1 M KCl solution [15]. GR(Cl^-) was taken at $Fe_4(OH)_8Cl \cdot nH_2O$. ⊕ indicates the conditions of corroding the iron coupons.

the electrochemical cell, indicating that the main part of the rust layer adhered to the iron substrate. In contrast, only the α-iron spectrum was obtained *in situ* for $E = -0.35\,V$ (not represented in Fig. 4); the rust layer did not adhere to the metallic surface and the corrosion products deposited in the bottom of the cell were analysed *ex situ* after filtration at room temperature under an inert N_2 atmosphere. The computer fittings, realised with Lorentzian-shape lines constrained to have the same width at half maximum, revealed the presence of two components in the first spectrum and six in the second one (Table 2). For $E = -0.55\,V$, the main component is the sextet of α-Fe. It is accompanied by a quadrupole doublet having hyperfine parameters characteristic of a ferrous compound. A value of $\Delta E_Q = 2.85\,mm\,s^{-1}$ is typical of ferrous hydroxide at room temperature [19, 26]. In contrast, for $E = -0.35\,V$, three sextets, S_1, S_2 and S_3, and three doublets, D_1, D_2 and D_3, are present. S_1 and S_2, characterised by large hyperfine fields H and nil ΔE_Q, can be attributed to magnetite Fe_3O_4 [31, 32]. S_3 owns a smaller hyperfine field and a negative ΔE_Q value of $-0.3\,mm\,s^{-1}$. It rather corresponds to poorly crystallised goethite [33, 34]. But the main part of the spectrum (72%) is due to the quadrupole doublets, two ferrous, D_1 and D_2, and one ferric, D_3. Such a spectrum, with ΔE_Q values around $2.2\,mm\,s^{-1}$ for the ferrous doublets, is typical of GR(Cl^-) at room temperature. In conclusion, the electrochemically induced corrosion products are those predicted by the Pourbaix diagram of Fig. 3 in the considered pH and $a[Cl^-]$ conditions.

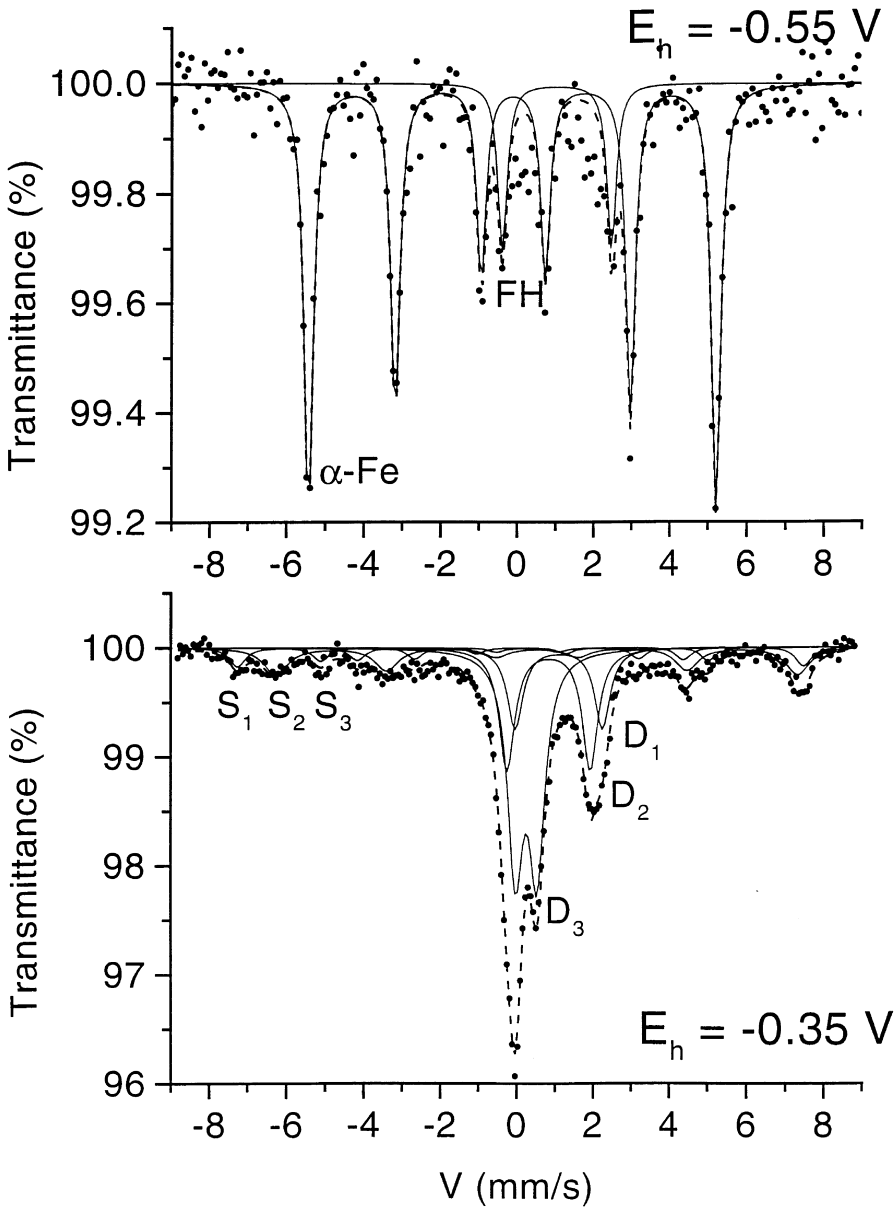

Fig. 4. Mössbauer spectra measured at room temperature of the electrochemically induced corrosion products of α-iron in a 1 M KCl solution of pH about 9, compared to that of standard GR(Cl^-). ··· experimental curve; ——— elementary quadrupole doublets; – – – global computed curve.

XRD analysis of GR(Cl^-)

The samples analysed by XRD are similar to sample 5 described above, and are thus constituted only of the GR compound. This is confirmed by the XRD pattern shown in Fig. 5 where not a single trace of ferric oxyhydroxide or magnetite is detected, which

Table 2. Mössbauer data at room temperature of the electrochemically induced corrosion products of α-iron in a 1 M KCl solution of pH about 9, compared with those of standard GR(Cl^-)

Spectrum obtained with $E = -0.55$ V ($FWHM = 0.29$)					Spectrum obtained with $E = -0.35$ V ($FWHM = 0.49$)				
	δ	ΔE_Q	H	RA		δ	ΔE_Q	H	RA
FH	1.20	2.85	0	15	D_1	1.25	2.27	0	21
α-Fe	0	0	331	85	D_2	0.98	2.17	0	14
					D_3	0.40	0.56	0	37
Standard GR(Cl^-) at RT$^{(+)}$ ($FWHM = 0.53$)					S_1	0.22	0	458	7
	δ	ΔE_Q	RA		S_2	0.65	0	422	16 ($FWHM = 0.74$)
D_1	1.22	2.34	29		S_3	0.23	−0.31	314	5
D_2	1.11	2.02	33						
D_3	0.35	0.58	38						

$^{(+)}$GR sample obtained by aerial oxidation of ferrous hydroxide, similar to sample 5 described previously. δ = isomer shift with respect to metallic α-iron in mm s^{-1}; ΔE_Q = quadrupole splitting in mm s^{-1} ; RA = relative abundance in %. Full widths at half maximum (FWHM), given in mm s^{-1}, are constrained to be equal for each Lorentzian-shape line.

indicates that the compound did not oxidise. However, some of the lines which are very broad overlap, especially at large angles. For this reason the interpretation of the spectrum was limited to the range 0–17° (θ). The relative intensities of the diffraction

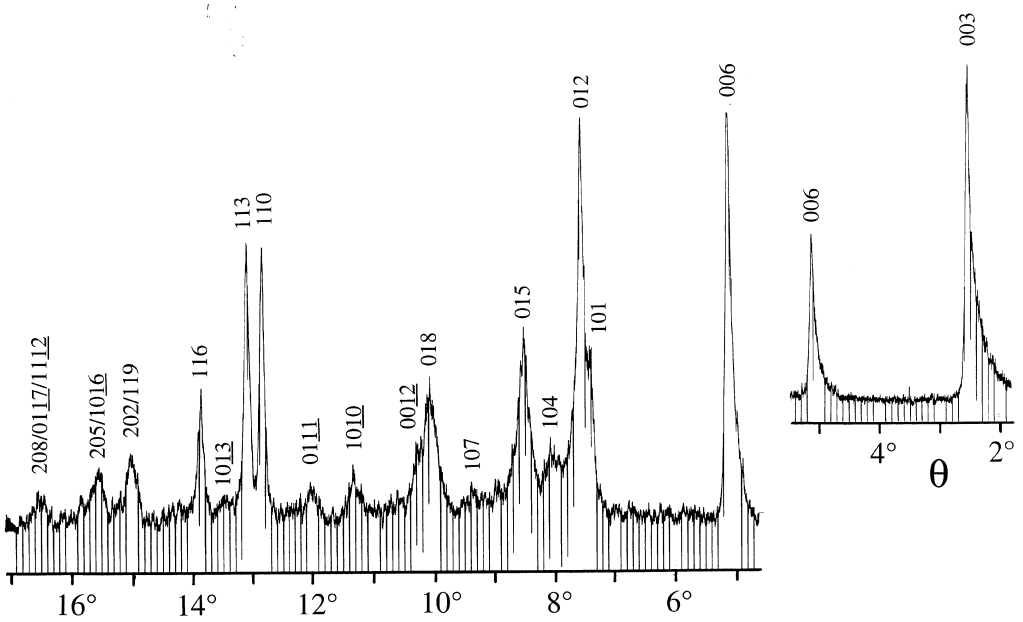

Fig. 5. X-ray powder diffraction pattern of GR(Cl^-). (MoKα_1 radiation, $\lambda = 0.070930$ nm).

lines were estimated by the 'Diffract AT' program. Observed interplanar distances and intensities are listed in Table 3.

DISCUSSION

Crystal structure of GR(Cl^-)

The crystal structures of GRs were assumed to be similar to that of the mineral pyroaurite [2, 35], $Mg_6^{II}Fe_2^{III}(OH)_{16}CO_3 \cdot 4H_2O$ as determined by Allmann [36] and Ingram and Taylor [37]. As demonstrated by the results listed in Table 3, a structural model derived from the pyroaurite structure, that is conserving its main features, can be reasonably proposed for GR(Cl^-). This model is derived from the crystal structure proposed for iowaite, the Mg(II)-Fe(III) pyroaurite-like mineral incorporating Cl^- ions [38]. Iowaite consists of hydroxide sheets $[Mg_3^{II}Fe^{III}(OH)_8]^+$, positively charged due to the trivalent Fe cations, which alternate regularly with negatively charged interlayers $[Cl \cdot 2H_2O]^-$ made of anions and water molecules. The rhombohedral structure cor-

Table 3. X-ray diffraction data (MoKα_1 radiation) compared with computed interplanar distances (nm) and intensities of GR(Cl^-). $a = 0.3190(1)$ nm and $c = 2.385(6)$ nm

hkl	d_{obs}	d_{calc}	I_{obs}/I_1	I_{calc}/I_1
003	0.797 (3)	0.7950	100	100
006	0.3966 (8)	0.3975	31.5	31.5
101	0.2744 (6)	0.2744		
012	0.2692 (4)	0.2691	34	30.8
009	0.264 (1)	0.2650		
104	0.253 (2)	0.2507	4.5	5.4
015	0.2392 (3)	0.2391	21	21.5
107	0.216 (2)	0.2146	2	3.0
018	0.2027 (3)	0.2026	19.2	21.4
0012	0.198 (1)	0.1988		
1010	0.1808 (4)	0.1805	5.5	6.3
0111	0.1702 (5)	0.1706	4.5	6.1
110	0.1595 (1)	0.1595	9.0	8.7
113	0.1563 (1)	0.1564	10.4	11.3
1013	0.1526 (7)	0.1528	5	3.9
116	0.1479 (1)	0.1480	4.3	5.9
0114	0.1448 (3)	0.1450	3	2.6
021	–	0.1379		
202	0.1375 (3)	0.1372	5	5.3
119	0.1364 (2)	0.1367		
024	0.1348 (3)	0.1346	1.5	0.8
205/0018	0.1323 (3)	0.1326	6	6.2
1016	0.1309 (4)	0.1312		
027	0.1284 (4)	0.1280	0.5	0.8
208/0117	0.1251 (2)	0.1252	5	3.8
1112	0.1240 (3)	0.1244		

responds to the OH^- layer sequence *AB BC CA* [Fig. 6(a)]. Mg and Fe atoms of the hydroxide layers are randomly distributed among the octahedral positions. The interlayers are mainly composed of Cl^- ions and oxygen atoms belonging to the water molecules which are extensively disordered and preferentially situated at about 0.040 nm off the threefold axis connecting two OH^- ions of adjacent hydroxide layers.

According to the chemical analyses performed on iowaite [38], there are approximately two water molecules per chloride ion, a value which was consequently admitted for GR(Cl^-). The composition of the sample studied here is then close to $Fe_{3.2}(OH)_{6.4}Cl \cdot 2H_2O$ (*cf.* discussion hereafter). The SHELXL-93 program was used to refine the various parameters (Table 4), allowing us to decrease the reliability factor $R_1 = \Sigma|F_{obs} - F_{calc}|/\Sigma F_{obs}$ down to 0.075. In contrast with the work of Braithwate *et al.* [38], Cl^- ions and water molecules were left free to occupy different sites, but this did not result in fundamental modifications. The fit improved with H_2O slightly closer to the OH-OH threefold axis than Cl^-, at 0.032 nm *vs* 0.080 nm [Fig. 6(b)]. It is consistent with the ionic radii of Cl^- and OH^- (0.181 *vs* 0.135 nm) [39] and the spacing of the

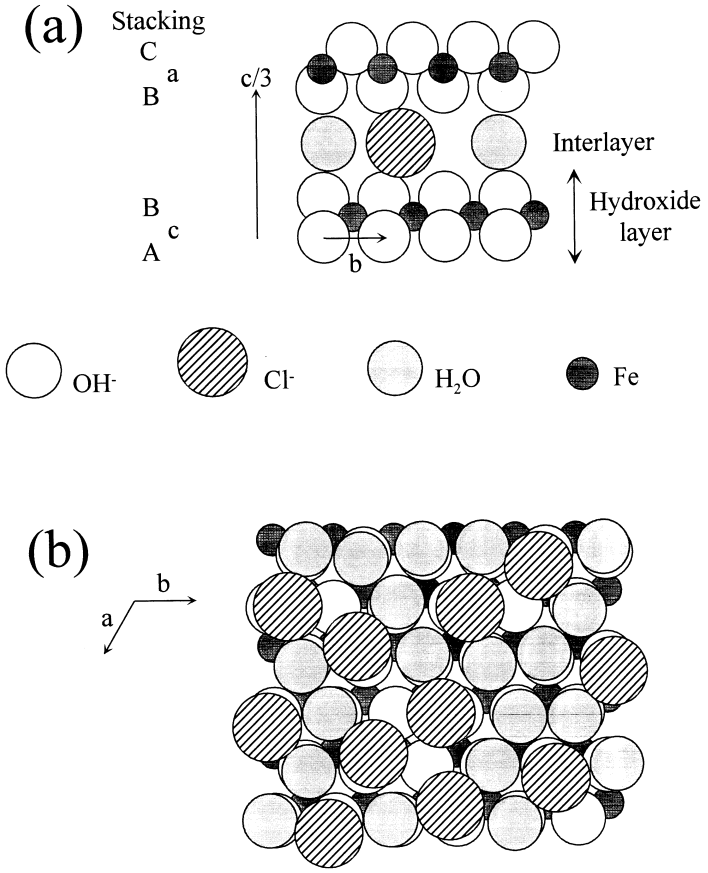

Fig. 6. Crystal structure of GR(Cl^-). (a) Stacking sequence. (b) Disposition of water molecules and chloride ions in an interlayer viewed along [001]. Only one interlayer, one OH^- and one Fe layer below it are represented.

Table 4. (a) Reduced coordinates of atoms in GR(Cl^-) and temperature factors

	x	y	z	U_{11}	U_{22}	U_{33}	U_{23}	U_{13}	U_{12}
Fe	0	0	0	0.009	0.009	0.025	0	0	0.0045
O (OH^-)	0	0	0.375	0.014	0.014	0.06	0	0	0.007
O (H_2O)	0.1	0.1	0.5	0.15	0.15	0.08	0.02	−0.02	0.1
Cl^-	0.25	0.25	0.5	0.3	0.3	0.08	0.02	−0.02	0.1

(b) Layer to layer and interatomic distances in nm

	Layer to layer distances	
Fe-OH^-: 0.099	OH^--OH^- in hydroxide layer: 0.199	OH^--interlayer: 0.298
	Interatomic distances	
Fe-OH^-: 0.209	OH^--OH^- (6): 0.319	OH^--OH^- (3): 0.277
OH^--H_2O: 0.300	OH^--Cl^-: 0.309	Cl^--H_2O (min.): 0.320

interlayers as revealed by the OH-Cl distance presented in Table 4 along with the other interatomic distances.

Composition and mechanisms of formation of GR(Cl^-)

The formation of GR(Cl^-) involves two reaction stages. In the first step which corresponds to the first thirty minutes, the redox potential varies only slightly, and the composition of GR(Cl^-) is constant. As demonstrated by Mössbauer spectroscopy, samples 1–3 keep the same Fe(II)/Fe(III) ratio close to 3, leading to formula $Fe^{II}_3Fe^{III}(OH)_8Cl\cdot nH_2O$ usually proposed for GR(Cl^-) [11–13]. It is also demonstrated that part of the GR is formed during precipitation, since 13% of the initial solid is made of GR. This is more likely due to the presence of dissolved oxygen in the solutions, which allows the formation of some Fe(III) during precipitation. This process is very similar to that observed during the coprecipitation from ferrous and ferric chlorides as described previously (*cf.* Fig. 2). Positively charged hydroxide layers containing Fe(III) cations would form initially before adsorbing anions, in this case Cl^-, and water molecules. These precursors would then merge alternatively during the growth of micro-crystals of GR(Cl^-). The same mechanism has been proposed during the formation and ageing of various hydroxides and hydroxy-salts, such as $Ni(OH)_2$ [40, 41].

In the second step of the reaction, the composition of GR(Cl^-) does not stay constant any more. The Fe(II)/Fe(III) ratio decreases continuously to reach a value of about 2.2. Such a variation was already observed [11, 13] and GR(Cl^-) compounds with Fe(II)/Fe(III) ratios down to 2 were reported to form in the presence of large chloride concentrations, about 2 to 4 mol l^{-1} [14]. The Mössbauer analysis of the various GR samples demonstrate that the hyperfine parameters of the various sites do not change during the reaction, except for the relative areas, which indicate that the various crystallographic sites do not change. This implies that the local environments of the Fe atoms are kept unchanged. According to Murad and Taylor who studied the mechanisms of oxidation of GR(CO_3^{2-}) by TMS [42, 43], new ferrous and ferric sites appear when the oxidation produces an excess of ferric ions, which is more likely due to the correlative

formation of O^{2-} ions replacing OH^- ions in the hydroxide sheets. Thus, the continuous oxidation of GR(Cl^-), which implies the decrease of the Fe(II)/Fe(III) ratio, is related to the continuous enrichment of the interlayers with chloride ions, the intercalation of one Cl^- leading to the loss of one electron, that is the oxidation of one Fe(II) into one Fe(III). This is confirmed by the chemical analyses performed by Schwertmann and Fechter [13] during the formation of GR(Cl^-), who observed that whereas the Fe(II)/Fe(III) ratio was decreasing from 3 to 2, the chloride concentration in solution was also decreasing, and the Fe(III)/Cl^- ratio staying close to 1 (*cf*. Fig. 1 from [13]). According to the crystal structure of the compound, it can be seen that such an *in situ* oxidation process can be considered.

A similar study concerning the formation and composition of Fe(II)-Fe(III) hydroxy-oxalate Green Rust, GR($C_2O_4^{2-}$), led to different results [21]; it was demonstrated that the composition of GR($C_2O_4^{2-}$) stayed invariant during the overall reaction, from the beginning of the oxidation of $Fe(OH)_2$ to the end of the oxidation of the GR, keeping a Fe(II)/Fe(III) ratio of 3. The work of Schwertmann and Fechter [13], devoted to GR(Cl^-) and GR(SO_4^{2-}), indicates similarly that the composition of GR(SO_4^{2-}) stays unchanged. Thus, the behaviour of GR(Cl^-) seems to be particular, likely due to the unique electric spherical charge permitting a gradual *in situ* intercalation forbidden for larger divalent anions, $C_2O_4^{2-}$ or SO_4^{2-}.

CONCLUSIONS

The mechanisms of formation of GR(Cl^-) are interpreted in relation with the crystal structure of the Fe(II)-Fe(III) hydroxy-chloride, which consist of $Fe(OH)_2$—like hydroxide sheets positively charged due to the presence of some Fe(III) cations, alternating with negatively charged interlayers made of Cl^- ions and water molecules. In slightly basic and chloride-containing aqueous media, GR(Cl^-) should be obtained as a corrosion product of iron and steels whether by oxidation of an initial ferrous hydroxide layer or by direct precipitation in the simultaneous presence of ferrous and ferric dissolved species. Potentiostatically induced corrosion of iron in such conditions confirmed the formation of GR(Cl^-) for potential values predicted by the corresponding *E vs* pH Pourbaix diagram.

Acknowledgements—The authors would like to thank Pr J. Protas and M. Lelaurain[1] for their expert assistance during the structural investigations.

REFERENCES

1. Butler, G. and Beynon, J.G., *Corros. Sci*., 1967, **7**, 385–404.
2. Stampfl, P.P., *Corros. Sci*., 1969, **9**, 185–187.
3. McGill, I. R., McEnamey, B. and Smith, D.C., *Nature*, 1976, **29**, 200–201.
4. Gancedo, J. R., Martinez, M. L. and Oton, J.M., *J. Physique* (*Colloq. C*6), 1976, **37**, 297–299.
5. Olowe, A. A., Bauer, P., Génin, J.-M.R. and Guézennec, J., *Corrosion NACE*, 1989, **45**, 229–235.
6. Génin, J.-M.R., Olowe, A. A., Benbouzid-Rollet, N. D., Prieur, D., Confente, M. and Résiak, B., *Hyp. Int*., 1991, **69**, 875–878.
7. Génin, J.-M.R., Olowe, A.A., Résiak, B., Benbouzid-Rollet, N.D., Confente, M. and Prieur, D., in *Marine*

[1] Laboratoire de Chimie du Solide minéral, Université H. Poincaré, Nancy, France.

corrosion of stainless steels: *chlorination and microbial effects*, European Federation Corrosion Series n° 10. The Institute of Metals, London, 1993, pp. 162–166.
8. Boucherit, N., Hugot-Le Goff, A. and Joiret, S., *Corros. Sci*., 1991, **32**, 497–507.
9. Boucherit, N., Hugot-Le Goff, A. and Joiret, S., *Mat. Sci. For*., 1992, **111-112,** 581–588.
10. Abdelmoula, M., Refait, P., Drissi, S. H., Mihé, J.-P. and Génin, J.-M.R., *Corros. Sci*., 1996, **38**, 623–633.
11. Detournay, J., Dérie, R. and Ghodsi, M., *Z. anorg. allg. Chem*., 1976, **427**, 265–273.
12. Refait, Ph. and Génin, J.-M.R., *Corros. Sci*., 1993, **34**, 797–819.
13. Schwertmann, U. and Fechter, H., *Clay Miner*., 1994, **29**, 87–92.
14. Refait, Ph. and Génin, J.-M.R., *Corros. Sci*., 1997, **39**, 539–553.
15. Refait, Ph., Bon, C., Bourrié, G., Trolard, F., Bessière, J. and Génin, J.-M.R., Determination of standard free enthalpy of formation of green rusts: Fe(II)-Fe(III) hydroxy-sulphate, -chloride and -carbonate. *Clay Miner*., submitted.
16. Pourbaix, M., *Atlas d'équilibres électrochimiques*. Gauthier-Villars, Paris, 1963.
17. Feitknecht, W. and Keller, G., *Z. anorg. Chem*., 1950, **262**, 61–68.
18. Bernal, J. D., Dasgupta, D. R. and Mackay, A.L., *Clay Min. Bul*., 1959, **4**, 15–30.
19. Miyamoto, H., Shinjo, T., Bando, Y. and Takada, T., *Bull. Ins. Chem. Res. Kyoto Univ*., 1967, **45**, 333–341.
20. Génin, J.-M.R., Abdelmoula, M., Refait, Ph. and Simon, L., Comparison of the green rust two lamellar double hydroxide class with the green rust one pyroaurite class: Fe(II)-Fe(III) sulphate and selenate hydroxides. *Hyp. Int*., in press.
21. Refait, Ph., Charton, A. and Génin, J.-M.R., Identification, composition, thermodynamic and structural properties of a pyroaurite-like Fe(II)-Fe(III) hydroxy-oxalate Green Rust. *Europ. J. Miner*., submitted.
22. Miyata, S., *Clays Clay Miner*., 1975, **23**, 369–375.
23. Miyata, S. and Okada, A., *Clays Clay Miner*., 1977, **25**, 14–18.
24. De Roy, A., Besse, J.-P. and Bondot, P., *Mat. Res. Bull*., 1985, **20**, 1091–1098.
25. Chanson, C., Fournès, L. and Grenier, J.-C., *C. R. Acad. Sc. Paris*, 1986, **303**, *serie II*, 1633–1636.
26. Génin, J.-M.R., Bauer, Ph., Olowe, A. A. and Rézel, D., *Hyp. Int*., 1986, **29**, 1355–1358.
27. Refait, Ph. and Génin, J.-M.R., *SIF Conference Proceedings*, 1996, **50**, 55–58.
28. Rézel, D., Bauer, Ph. and R Génin, J.-M., *Hyp. Int*., 1988, **42**, 1075–1078.
29. Jolivet, J.-P., Belleville, P., Tronc, E. and Livage, J., *Clays Clay Miner*., 1992, **40**, 531–539.
30. Génin, J.-M.R., Refait, Ph., Simon, L. and Drissi, S.H., *Hyp. Int*., 1998, **111**, 313–318.
31. Bauminger, R., Cohen, S. G., Marinov, A. and Ofer, S., Segal, E., *Phys. Rev*., 1961, **122**, 1447–1450.
32. Olowe, A. A., Pauron, B. and Génin, J.-M.R., *Corros. Sci*., 1991, **32**, 985–1001.
33. Murad, E., *Miner. Mag*., 1979, **43**, 355–361.
34. Olowe, A. A. and Génin, J.-M.R., *Corros. Sci*., 1991, **32**, 965–984.
35. Allmann, R., *Chimia*, 1970, **24**, 99–108.
36. Allmann, R., *Acta Cryst*., 1968, **B24**, 972–977.
37. Ingram, L. and Taylor, H.F.W., *Min. Mag*., 1967, **36**, 465–479.
38. Braithwate, R. S. W., Dunn, P. J., Pritchard, R. G. and Paar, W.H., *Mineral. Mag*., 1994, **58**, 79–85.
39. Shannon, R.D., *Acta Cryst*., 1976, **A32**, 751–767.
40. Longuet-Escart, J. and Méring, J., *J. Chim. Phys*., 1954, **51**, 440–445.
41. Bagno, B. and Longuet-Escart, J., *J. Chim. Phys*., 1954, **51**, 434–439.
42. Murad, E. and Taylor, R.M., *Clay Min*., 1984, **19**, 77–83.
43. Murad, E. and Taylor, R.M., *Ind. Appl. of Mössb. Effect*, *Hyp. Int*., 1986, **29**, 585–593.